For Submission to Journal of Neurophysiology

RECRUITMENT IN RETRACTOR BULBI MUSCLE DURING EYEBLINK CONDITIONING: EMG ANALYSIS AND COMMON-DRIVE MODEL

N. F. Lepora[1], J. Porrill[1], C. H. Yeo[2], C. Evinger[3], and P Dean[1]

[1]*Department of Psychology, Sheffield University, Sheffield, United Kingdom.*

[2]*Department of Anatomy and Developmental Biology, University College London, London, United Kingdom*

[3]*Department of Neurobiology and Behavior, State University of New York, Stony Brook, New York*

Running Head: Recruitment in Eyeblink Conditioning

Correspondence to: Paul Dean, Department of Psychology, University of Sheffield, Western Bank, Sheffield S10 2TP, U.K.

E-mail: p.dean@sheffield.ac.uk

Phone: +44 114 222 6521

Fax +44 114 276 6515

ABSTRACT

In analyzing the role of the cerebellum in classical conditioning of the eyeblink and nictitating membrane (NM) response, the control of conditioned response dynamics is not well understood. Previous studies suggested that the control signal is linearly related to the conditioned response as a result of recruitment within the accessory abducens motoneuron pool, which acts to linearise retractor bulbi muscle and NM response mechanics [Lepora, 2007 #8710]. Here we investigate possible recruitment mechanisms.

Data came from simultaneous recordings of NM position and multi-unit electromyographic (EMG) activity from the retractor bulbi muscle of rabbits during eyeblink conditioning in which tone and periocular shock act as conditional and unconditional stimuli, respectively. Action potentials (spikes) were extracted and classified by amplitude. Firing rates of spikes with different amplitudes were analyzed with respect to NM response temporal profiles and total EMG spike firing-rate.

Four main regularities were revealed and quantified: (i) spike amplitude increased with response amplitude; (ii) smaller spikes always appeared before larger spikes; (iii) subsequent firing rates co-varied for spikes of different amplitude, with smaller spikes always firing at higher rates than larger ones, (iv) firing-rate profiles were approximately Gaussian for all amplitudes.

These regularities suggest that recruitment does take place in the retractor bulbi muscle during conditioned NM responses, and that all motoneurons receive the same command signal (common-drive hypothesis). To test this hypothesis, a model of the motoneuron pool was constructed in which motoneurons had a range of intrinsic thresholds distributed exponentially, with threshold linearly related to EMG spike amplitude. Each neuron received the same input signal as required by the common-drive assumption. This simple model reproduced the main features of the data, suggesting that conditioned NM responses are controlled by a common drive mechanism that enables simple commands to determine response topography in a linear fashion.

INTRODUCTION

Classical conditioning of the rabbit's nictitating membrane (NM) response has been extensively studied in two contexts, first as an exemplar of associative learning [e.g. \Gormezano, 1983 #3190;Dudeney, 2007 #8786], and more recently as a suitable task for investigating cerebellar function in the production of a learned movement [e.g. \Hesslow, 2002 #7004;Thompson, 2005 #8399]. Although a major attraction of using the NM response has been its apparent simplicity, accumulating evidence suggests that this simplicity is only relative. For example, while the NM response does indeed have much simpler mechanics than those of limb movement, accurate control of NM position and velocity is still not a straightforward problem. The rabbit NM response is produced by retraction of the globe into the orbit, which displaces Harder's gland to force the NM across the cornea [Eglitis, 1964 #8013]. Globe retraction is produced primarily by the retractor bulbi muscle, which is innervated by motoneurons in the accessory abducens nucleus [Disterhoft, 1985 #3174]. Restoration of globe and NM position depends upon relaxation of the retractor bulbi muscle and the elastic properties of the globe, the NM, and surrounding tissues, rather than the action of an antagonist muscle. This quite complex chain of events linking motoneuron firing to NM movement suggests on *a priori* grounds that the relation between the two will not be simple [e.g. \Delgado-García, 2005 #7992].

To examine these relationships explicitly Bartha and Thompson [, 1992 #1702;, 1992 #1698] constructed a detailed model of the rabbit NM response, which incorporated the mechanics of the globe, Harder's gland, the NM, and the motor units of the retractor bulbi muscle. Subsequent reimplementation of this model to examine the relation between motoneuron firing and NM response parameters [Mavritsaki, 2007 #8358] found that model performance depended critically upon the nature of motoneuron recruitment (that is, upon the relationship between the number of motoneurons firing and the muscle force). When there were no recruitment and all motoneurons fired with the same rate (rate-coding of muscle force), as investigated by Bartha and Thompson [, 1992 #1698;, 1992 #1702], then maximum NM displacement had a complex, sigmoidal relation to firing rate, reflecting the properties of retractor bulbi motor units [Lennerstrand, 1974 #5589]. If however rate coding were combined with appropriate recruitment of motor units, peak NM amplitude and total motoneuron pool firing had a simple linear relation over the normal range of NM response amplitudes.

The question of how far this linearity is found in practice was addressed by analyzing EMG records from the retractor bulbi muscle during the production of conditioned NM responses [Lepora,

2007 #8710]. Spikes were extracted from the EMG record and the relationship of their firing rate to the NM response parameters was examined. Two relations were evident from this analysis: (1) the temporal profile of EMG spike rate is well-approximated a Gaussian function, with the peak amplitude of this Gaussian linearly related to the peak amplitude of the conditioned response; (2) the NM response profiles could be generated from the corresponding total EMG spike-rate profiles by passing the latter through a linear first order linear differential equation equivalent to a simple first-order filter with time constant of order 100-200ms. Over acquisition of the conditioned response, the peak EMG spike-rate increased appropriately to drive a larger peak NM response, while the time-to-peak of the EMG spike-rate and NM response amplitude did not change appreciably.

Therefore the overall effective dynamics linking motoneuron firing to NM movement can be viewed as a 'plant simplification' that make conditioned response parameters such as amplitude, duration and timing much easier to control than the complexities of the plant (i.e. muscle plus globe) would at first suggest. Such a linearised 'virtual plant' should result in a lower computational load in the neuronal systems involved in driving the movement and give more accurate motor control. Similar plant simplifications appear to be a widespread phenomena in physiological motor control [Angelaki, 2004 #7442;Mussa-Ivaldi, 1994 #8576;Nichols, 1976 #7889], so the mechanisms by which they are achieved are of general interest.

Our previous analysis, which treated all EMG spikes as equal irrespective of their amplitude [Lepora, 2007 #8710], cast no direct light on the underlying mechanism. Here we extend the analysis to take spike amplitude into account, because inspection of retractor bulbi EMG records strongly suggested that spike amplitude and conditioned response parameters were related. Such a relation implies recruitment, and indeed the analysis of EMG spike-amplitudes indicated a simple procedure for recruiting motor units in the retractor bulbi muscle in order to control CR amplitude. The same command is sent to all motoneurons in the accessory abducens nucleus pool. Its intensity varies over time with a Gaussian profile, whose peak is related to CR amplitude and width to CR duration. Motoneuron threshold varies with EMG spike amplitude, so that the higher the threshold, the larger the spike. Spike amplitude varies, in turn, with motor unit strength. In this manner, a simple high-level command can generate the forces necessary for the appropriated sized CR, using the common-drive mechanism for motor control previously proposed for a range of movements using that employ other muscles [De Luca, 1982 #9122;De Luca, 1982 #9123;Masakado, 1995 #9137;Jabre, 1996 #9121;De Luca, 1996 #3706;Sauvage, 2006 #8496].

In these previous studies, EMG records allowed identification of the action potentials from individual motor units, so that unit firing rate could be unequivocally related to the amplitude of its action potential. Here, in contrast, the technical difficulties of recording from the small and mobile retractor bulbi muscle prevent individual motor unit action potentials from being reliably identified. In order to determine whether the common-drive mechanism could in principle account for the EMG patterns observed in the previous study, we attempted to simulate the data patterns using a computational model. This model was able to characterize various observed features of the EMG records from some common assumptions about motoneurons undergoing common-drive. The resulting evidence for a common-drive mechanism is consistent with the view that because of the technical difficulties of EMG recording and analysis "computational models are fast becoming the dominant means to establish the mechanism relating EMG to muscle force and neural drive" [Keenan, 2007 #9106`, p.1581].

Some of the findings have appeared in abstract form [Lepora, 2006 #8429].

METHODS

Data Collection

Procedures for surgery, training, and data acquisition have been described previously [Lepora, 2007 #8710]. Briefly, data were obtained from two different laboratories, one at University College London (Yeo) and the other at the State University of New York at Stony Brook (Evinger).

At University College London, EMG electrodes were implanted in the retractor bulbi muscle of three male Dutch belted rabbits (2.0-2.2 kg), subsequently referred to as RB1-3, under halothane general anesthesia. All general surgical procedures were as described in Yeo, Hardiman and Glickstein [, 1985 #3167] and those specific to the EMG electrode implantation are as previously described in detail (Lepora et al 2007). EMG electrodes were of Teflon-coated stainless steel wire (50 μm diameter bare). In subject RB1, a pair of additional EMG electrodes, similar to those used in the retractor bulbi muscle, were implanted in the orbicularis oculi muscle immediately dorsal to the upper eyelid at a spacing of approximately 3 mm. Postoperatively, all subjects received buprenorphine twice per day for three days to provide post-implant analgesia and minimize discomfort. Displacement of the NM was measured with an isotonic transducer based on a low-torque potentiometer [Gruart, 1995 #2361] whose output was fed into an analogue-to-digital converter (CED 1401). For adaptation and training, each subject was placed in a restraining box in a sound-attenuating chamber facing a centrally mounted loudspeaker, and the NM transducer fitted. In the 50 min adaptation session, no stimuli were presented. For acquisition, the conditioned stimulus (CS) was a 1 kHz sinusoidal tone of intensity 85 dbA and duration 560 ms (RB1) or 410 msec (RB2, RB3), delivered through the loudspeaker. The unconditioned stimulus (US) was a 60 ms train of 3 biphasic current pulses of 2 mA delivered to the periorbital region. The inter-trial interval between CS presentations varied randomly between 25 and 35 s, and 100 trials were presented each session. On every 10th trial the CS was presented alone. On each trial EMG and NM response data were recorded for a 2 sec period starting 1 sec before CS onset. EMG data were sampled at 5-40 kHz and NM response data at 1kHz. After acquisition, RB1 and RB2 were tested with triplets, which were repeating sets of one trial CS alone, one trial CS+US, and one trial US alone. In addition, RB1 was tested with varying CS intensities (65, 75, 85 and 95 dBA).

General surgical procedures at the Stony Brook University laboratory were identical. To insert EMG electrodes, a pair of Teflon-coated stainless steel wires (76 μm diameter bare, 140 μm coated, A-M Systems #791000) were inserted into one slip of the retractor bulbi with a 30 gauge hypodermic needle. Five hundred microns of insulation was removed from the tip of each wire and tip separation between the wires was between 1 and 2 mm. To eliminate any postoperative discomfort, rabbits received buprenorphine twice daily for two days after the surgery. Data were analysed from rabbit (RB4), a New Zealand white.. After initial acquisition of the conditioned response, RB4 was tested under a variety of conditions, including variations in CS and US intensity, and extinction.

Data Selection

The data used for analysis came from trials in which the CS was presented on its own, and CR amplitude was >2.5% of the maximum CR amplitude for that subject. About 15% of these trials were subsequently discarded either (i) because there was spontaneous movement of the NM just before CS presentation, or (ii) there was interference in the EMG or NM response signals, or there was evidence from the EMG recording suggesting electrode movement during the CR.

Data Analysis

Figure 1 about here

The occurrence of motor-unit action potentials was estimated from spikes in the EMG records [Sanders, 1996 #6718] using a threshold crossing procedure so that a spike was registered whenever EMG amplitude increased past a minimum spike amplitude threshold θ (Fig 1A). Given an EMG signal $\boldsymbol{x} = (x_0, x_1, x_2, \ldots)$ sampled at frequency f_{EMG} Hz, [i.e. at discrete time $t_{\mathrm{EMG}} = (0, 1/f_{\mathrm{EMG}}, 2/f_{\mathrm{EMG}}, \ldots)$], this procedure gives a spike sequence $\boldsymbol{s}$ that is a binary time series of zeros and ones

$$\mathbf{s} = \left(s_0, s_1, s_2, \cdots\right), \qquad s_i = \begin{cases} 1, & x_i < \theta < x_{i+1}, \\ 0, & \text{otherwise.} \end{cases} \tag{1}$$

Possible problems with this method were discussed in a previous analysis of the same EMG dataset [Lepora, 2007 #8710]. First, high-frequency noise can cause multiple-spike counting artifacts, so the EMG records were down-sampled to a frequency of 5kHz. Secondly, at high spiking rates there can be significant spike overlap, producing a wave-like interference pattern rather than discrete action potentials [Sanders, 1996 #6718]. The effects of this interference were demonstrated to be minor for

the EMG datasets under consideration [Lepora, 2007 #8710]. Thirdly, a suitable threshold θ must be chosen for each subject. A signal-to-noise separation procedure was used to estimate the values for θ, which are reproduced here in Table 1 for each of the 4 subjects RB 1-4.

Table 1 about here

As explained in the Introduction, the focus of the present study is EMG spike amplitude. The distribution of spike amplitudes was quantified by placing the peak amplitude ε of each of the spikes found by equation (1) in one *of* N_{class} distinct spike amplitude classes. These classes were defined from a set of equally-spaced thresholds $\theta_1 < \theta_2 < ... < \theta_{N_{class}}$, such that a spike of amplitude ε is in class k (where $1 \le k \le N_{\text{class}}$) if

$$\text{Class } k: \qquad \theta_{k-1} < \varepsilon \le \theta_k, \qquad \theta_k = \theta_0 + k\frac{\varepsilon_{\max} - \theta}{N_{\text{class}}}, \tag{2}$$

where θ_0 is the spike-detecting threshold used in equation (1) and ε_{max} is the maximal spike amplitude across all EMG records under consideration (values for ε_{max} are given for RB 1-4 in Table 1). A characteristic amplitude $\overline{\varepsilon}_k$ for the spikes in each amplitude class is the midpoint of their range

$$\overline{\varepsilon}_k = \left(\theta_{k-1} + \theta_k\right)/2. \tag{3}$$

The above procedure results in N_{class} spike sequences $\left(s_0^{(k)}, s_1^{(k)}, s_2^{(k)}, ...\right)$, with each a binary time series of whether spikes occur in a particular amplitude range—for example, with N_{class} = 5 classes, the spike classes k=1,3,5 can be thought of as signaling when the 'small', 'medium' and 'large' spikes occur, as illustrated in Fig. 1. It is important to note that these classes are a convenient measure for dividing spikes by amplitude along a continuum of values, rather than representing true clusters of spikes into distinct classes.

Once spikes had been extracted, their firing rates were calculated from the number of spikes in successive 50-ms time intervals. The noise levels of individual records meant that data had to be pooled across trials, based on similarity of CR amplitude. Three-trial batches were typically used [Lepora, 2007 #8710] to give a suitable number of spikes for analysis, with the trials ordered by peak NM amplitude to ensure that similarly sized conditioned responses were averaged over. All results in this paper were checked for robustness with respect to 5, 6, 7, 8, 9 and 10 classes, and results were not found to change appreciably apart from a general deterioration of the results as the number of

classes was increased because of too few spikes in each class. For simplicity, therefore, the number of spike classes was always set to N_{class} = 5, a value small enough for the results to have enough spikes in each class and large enough for statistical analysis of the EMG records with respect to spike height.

Previous analysis of the EMG data indicated that for conditioned responses a portion of the total-spike rate profiles could be well fitted by Gaussian curves [Lepora, 2007 #8710] according to the equation

$$f(t) = h \exp\left[\frac{-(t-\mu)^2}{2\sigma^2}\right], \tag{4}$$

where *f(t)* is instantaneous firing rate calculated over successive 50 ms intervals, μ is the time of the distribution mean, *h* its maximum amplitude and σ a measure of its width. Fitting was restricted to the interval from CS onset to one ISI after US onset (ISI = inter-stimulus interval, the time between CS- and US-onsets), to exclude a tail in the spike rate profile of some records. This range actually covers most of the spike rate variation of each record, because the peak frequency typically occurs significantly before US onset (see Fig. 2, for example). Effectively, this procedure characterized each spike distribution by three parameters estimated from the firing rate dataset as follows. The mean μ is the time-weighted mean of the spike rate,

$$\mu = \frac{1}{N}\sum_{j=0}^{n} f_j\, t_j, \qquad N = \sum_{j=0}^{n} f_j = \frac{1}{\delta}\sum_{j=0}^{n} s_j, \tag{5}$$

where f_j represents the firing rate of the *j*th bin from a total of *n* bins, t_j is the time at which that firing rate occurs and *N* is the total number of spikes divided by the time-width δ of the bin. The maximum amplitude *h* is the peak value across the spike rate record. The width σ is found by equating the spike total of the record to that for the Gaussian curve (*i.e.* matching areas under the curves) through the relation

$$\sigma = \frac{1}{h\sqrt{2\pi}}\int_{t=0}^{2} \exp\left(-\frac{(t-\mu)^2}{2\sigma^2}\right) dt = \frac{1}{h\sqrt{2\pi}}\sum_{j=0}^{n} f_j\,\delta = \frac{N\delta}{h\sqrt{2\pi}}. \tag{6}$$

The goodness of fit for the function in equation (4) is then the R^2 value

$$R^2 = 1 - \frac{\sum_{j=0}^{n}\left(f_j - f\left(t_j\right)\right)^2}{\sum_{j=0}^{n}\left(f_j\right)^2}, \tag{7}$$

which describes the proportion of variance accounted for by the fit of *f(t)* to the spike rate data.

Here we also applied this Gaussian-fitting analysis to the firing rate profiles of the different EMG spike amplitude classes according to

$$\overline{f}_k(t) = h_k \exp\left[\frac{-\left(t-\mu_k\right)^2}{2\sigma_k^{\,2}}\right], \tag{8}$$

where $\overline{f}_k(t)$ is the firing rate of class *k*. This results in a set of three parameters (μ_k, σ_k, h_k) describing the spike distribution of each of the N_{class} spike amplitude classes, with a fitting parameter r_k^2 describing the goodness of fit.

Finally, the relationships between the values for instantaneous total firing rate *f(t*) and the class firing rates $\overline{f}_k(t)$ were analyzed for each data set. It proved possible to fit these relations with straight lines of the form

$$\overline{f}_k(t) = g_k\left[\, f(t) - \overline{b}_k \,\right]^+ \tag{9}$$

where g_k is the gradient of the best-fit line for spike amplitude class *k*, $\overline{b}_k$ is the base total-spike rate representing the intercept above which $\overline{f}_k(t)$ is greater than zero, and the operation $[x]^+$ truncates its argument to positive values.

Simulation of EMG Data by Common-Drive Mechanism

Figure 2 about here

The basic structure of the motoneuron-pool model is shown in Fig. 2. Motoneurons in the accessory abducens nucleus were represented individually. Each motoneuron had its own threshold and gain, but was driven by an input common to all the motoneurons. EMG spike amplitude was related to motoneuron threshold, so that modeled EMG records could be simulated and then analyzed in the same way as the actual EMG records. The model is a simplified version of EMG models described previously [e.g. \Fuglevand, 1993 #3371;Zhou, 2004 #8105;Keenan, 2006 #8294;Keenan,

2007 #9106], with the additional features of (i) a Gaussian-profile common drive, and (ii) a grouping of motoneuron outputs on the basis of EMG-spike amplitude.

The model is first described with parameters appropriate for dataset RB1. The manner in which parameters were varied to fit the other data sets (RB2-4), and then to test model robustness, are described subsequently.

Gaussian-Profile Common Drive

Analysis of EMG spikes recorded from the retractor bulbi muscle during the production of a set of conditioned responses at various stages through conditioning indicates that their overall firing rate has a temporal profile that is approximately Gaussian in shape [Lepora, 2007 #8710]. Accordingly, the common-drive input current *I(t)* to each motoneuron was given a Gaussian profile

$$I(t) = I_0 \exp\left[\frac{-(t-\mu)^2}{2\sigma^2}\right], \qquad (10)$$

where μ is the time at which the current reaches its peak amplitude I_0, and σ is the width of the Gaussian function. The parameters μ and σ are independent of the amplitude of the conditioned response, whereas I_0 is assumed to be directly proportional to the peak amplitude of the conditioned-response [Lepora, 2007 #8711].

Parameter values for μ and σ were taken directly from the EMG-spike firing rates for dataset RB1, giving μ = 0.43 sec and σ = 0.14 sec (values given in Figs 6A,B). However the third parameter I_0 is not specified by available measurements, and so has to be initially assigned a plausible value. Given the maximum possible NM response amplitude is 15 mm [references in \Mavritsaki, 2007 #8358], a numerically convenient value for the I_0 corresponding to that response is 15 nA. The maximum value of I_0 (= I_{max}) for a given dataset is then simply determined by the amplitude of the maximum conditioned response in that dataset. For RB1 this was 4 mm, giving I_{max} = 4 nA.

Properties of Motoneuron Pool

The method for calculating the firing rate of a motoneuron given its synaptic input current and intrinsic properties was taken from previous simplified motoneuron models [Heckman, 1990 #1417;Binder, 1993 #1961;Dean, 1997 #4171]. These models assume that an individual motoneuron

starts to fire when its intrinsic threshold current, termed the rheobase *R,* is exceeded by the effective synaptic current *I(t)*. Instantaneous firing rate *f(t)* for a motoneuron then given by:

$$f_i(t) = G_i\left[I(t) - R_i\right]^+, \tag{11}$$

where G_i is a constant representing the intrinsic gain of the motoneuron as indicated by the slope of the relation between firing rate and injected current [Binder, 1993 #1961], and the notation $[x]^+$ corresponds to x for $x>0$ and 0 for $x\leq 0$; the index i labels the motoneuron and ranges between one and the total number of motoneurons n_{MN} (here set to 100, from observations in cat [\Lennerstrand, 1974 #5589]).

In accordance with previous studies [Fuglevand, 1993 #3371;Zhou, 2004 #8105;Keenan, 2007 #9106] the gains G_i were assumed to be the same (= *G)* for all motoneurons [cf. properties of abducens motoneurons as discussed in \Dean, 1997 #4171], and the thresholds R_i varied so as to give many low threshold motoneurons and progressively fewer high threshold motoneurons. An exponential distribution is convenient for this purpose

$$R_i = R_{\max}\frac{e^{q(i-1)/(n_{MN}-1)}-1}{e^q-1}. \tag{12}$$

where $R_{\max}$ is the maximum threshold and the exponent q defines the proportion of small to large rheobase currents.

The combined values for G and R_{max} are constrained by the previous assignment of 15 nA for the value of the input current that produces the maximum possible NM extension of 15 mm. For the initial model R_{max} was set to 7.5 nA. The last recruited neuron thus starts to fire at this value of input current, and must reach its maximum effective firing-rate when the input current reaches 15 nA, i.e. over a range of 7.5 nA. Since the isometric forces produced by motor units in the retractor bulbi muscle saturate at stimulation frequencies of ~150 spikes/sec [Lennerstrand, 1974 #5589], motoneuron gain G must be 20 spikes/s/nA. This can be compared with measured values of 20-40 Hz/nA for cat abducens motoneurons [Grantyn, 1978 #1523]. Finally, q in equation (12) was assigned the value of 3.45 by trial and error. The relation of this parameter to EMG properties was explored subsequently (details below).

Figure 3 about here

The properties of the model motoneuron-pool produced by equations (11) and (12) with these parameters are shown in Fig. 3. Because equation (12) describes an exponential relation between motoneuron number and threshold (Fig. 3A), the actual distribution of motoneuron thresholds is hyperbolic (Fig. 3B). This distribution produces a relationship between input current and total pool firing-rate that is close to linear over the range of inputs currents for the RB1 dataset (Fig 3D).

EMG Generation

Simulated EMG records were generated from model firing-rate profiles as follows. The shapes of the individual EMG spikes, and possible interference between spikes, were ignored, since analysis of the actual EMG records for the retractor bulbi muscle suggested that for the data under consideration interference effects were not important [Lepora, 2007 #8710]. The relationship between spike amplitude and motoneuron threshold was assumed to be linear.

$$\varepsilon_i = \theta_0 + \frac{\varepsilon_{\max} - \theta_0}{I_{\max}} R_i \tag{13}$$

where ε_i is the height of spike produced by the i-th motor unit, θ_0 is the threshold height for spikes to be counted, ε_{max} the maximum possible spike height, and I_{max} is the maximum input current for the RB1 dataset. Finally, a sampling parameter $0<p<1$ was introduced to convert summed motoneuronal firing to summed EMG-spike firing

$$f(t) = p\sum_{i=1}^{n_{MN}} f_i(t). \tag{14}$$

In the absence of any prior evidence on the motor units sampled, it was assumed that the subsample of measured units was unbiased across the motoneuron pool, given the small size of the retractor bulbi muscle, so that p can be regarded as a constant for any given dataset of EMG records.

For the RB1 dataset θ_0 = 0.17mV, ε_{max} is the maximum observed spike height of 2.53 mV, and I_{max} = 4 nA. These parameters give the linear relation between spike amplitude and motoneuron threshold depicted in Fig. 3C. The sampling fraction p was set to 0.09, determined by the ratio of the observed peak EMG firing rate (440 spikes/sec) to the summed model firing rate for RB1's largest conditioned response (peak amplitude 4mm).

Fitting Data Sets RB2-4

A subset of model parameters was varied in order to fit the remaining three datasets RB2-4. These were the parameters I_0 ,μ and σ for the Gaussian-profile common drive (equation (10)), the parameter q for the distribution of motoneuron thresholds (equation (12)), and the EMG parameters θ_0, ε_{max} and p (equations (13) and (14)). Appropriate values of these parameters gave fits to the datasets RB2-4 similar to those shown for dataset RB1. Fits for subjects RB1 and RB4 are shown in RESULTS (Figs 6-8) and fits for subject RB2 and RB3 in supplementary material (Figs S1-S3).

(i) Experimentally determined EMG threshold θ_0 = 0.15 mV, 0.0275 mV, 0.0375 mV and maximum EMG spike height $\varepsilon_{\max}$ = 0.75, mV 0.67 mV, 0.36 mV for datasets RB2-RB4 (Table 1). Overall model behavior is unaffected by changing these parameters because the class- and total-firing rates do not depend on these EMG parameters (both the spike amplitudes and class boundaries are scaled identically, so the motor units remain in the same classes.)

(ii) The Gaussian mean μ and width σ of the common drive current were set equal to the corresponding values for the mean and intercept width of the data for RB2-RB4, which are μ = 0.28 sec, 0.35 sec, 0.31 sec and σ = 0.10 sec, 0.11 sec, and 0.10 sec respectively (Figs 7 and 8). Because the model equations (10) to (14) depend *implicitly* on time, the model output remains of the same functional form in relations (16) and (17) but with the precise temporal profiles rescaled by the changes to the model input, or common drive current.

(iii) The motoneuron sampling proportion p is fixed to the peak model firing rate; peak firing rates for datasets RB2-RB4 are 220 sp/s, 450 sp/s and 370 sp/s (see Table 1), giving p values of 0.14, 0.10 and 0.053 respectively. Overall model behavior is again robust to changing the sampling proportion because only the absolute firing rates are affected, not the functional form of relations (16) and (17).

(iv) The parameter q specifies the precise exponential relation between motoneuron number and threshold (equation (12)), and its value determines the parameters u, v in relations (16) and (17) (see also Figs 7 and 8) in a complicated manner that depends on the EMG threshold θ_0 and maximum EMG spike height $\varepsilon_{\max}$. Appropriate values of q were determined by trial and error for the datasets RB2-4, giving 1.8, 4.4 and 1.9 (see also robustness below).

Parameter Variation: Model Robustness

Parameters were subsequently varied systematically to investigate the robustness of the model. For this purpose the appropriate parameters were those describing model structure in equations (11) and (12). Non-linear relations between EMG spike amplitude and rheobase current were also considered, for example exponential and power laws, but no significant improvement to model performance was achieved for the corresponding increase in model complexity.

Glossary

CS Conditioned stimulus

US Unconditioned stimulus

CR Conditioned response

UR Unconditioned response

EMG Electromyogram

MN Motoneuron

MU Motor unit

MUAP Motor unit action potential

NM Nictitating membrane

RB Retractor bulbi

$\bar{b}_k$ base total-spike rate at which f_k becomes greater than zero

c_i strength of motor unit *i*

$f(t)$ total instantaneous EMG spike firing rate at time *t*

$f_i(t)$ instantaneous firing rate of model neuron *i* at time *t*

$\bar{f}_k(t)$ instantaneous firing rate of spike amplitude class *k* at time *t*

f_{EMG} EMG sampling frequency

g_k gradient of best-fit line for spike amplitude class *k*

G_i intrinsic gain of a motoneuron

h_k maximum of Gaussian-fit to firing rate for class *k*

$I(t)$ common drive input current

I_0 peak input current for a single trial

$I_{\max}$ maximum input current for dataset

k spike amplitude class

l gradient of firing rate width σ_k with EMG amplitude $\overline{\varepsilon}_k$

m gradient of base firing rate b_k with EMG amplitude $\overline{\varepsilon}_k$

n number of time-bins in fit to spike rate

n_{MN} total number of motoneurons in the pool

N number of EMG spikes divided by width δ of time-bin in fit to spike rate

N_{class} number of spike amplitude classes

p proportion of sampled motoneurons

q exponent defining the proportion of small to large rheobase currents R_i

r^2 square of correlation coefficient

R_i rheobase current of a motoneuron

$R_{\max}$ highest rheobase current in motoneuron pool

s exponent defining the proportion of small to large motor unit strengths c

t time

t_{EMG} times when EMG sampled

u exponent of peak firing rate h_k with EMG amplitude $\overline{\varepsilon}_k$

v exponent of gradient g_k with EMG amplitude $\overline{\varepsilon}_k$

δ width of time-bin in fit to spike rate

$\varepsilon_{\max}$ maximum EMG spike amplitude

$\overline{\varepsilon}_k$ EMG amplitude in midpoint of range for class k

θ_0 EMG threshold for spike detection

θ_k EMG threshold for spike detection in the spike amplitude class number k

μ mean time of Gaussian-fit to total-firing rate $f(t)$

σ width of Gaussian-fit to total-firing rate $f(t)$

μ_k mean time of Gaussian-fit to firing rate $f_k(t)$ for class k

σ_k width of Gaussian-fit to firing rate $f_k(t)$ for class k

RESULTS

Analysis of EMG Data

For clarity, the data analysis and modelling results (Figs 6-8) are presented here for only two of the four subjects: RB1 (a Dutch belted rabbit) and RB4 (a New Zealand white). The corresponding results for the remaining two subjects RB2 and RB3 (both Dutch belted rabbits) are shown in supplementary material (Figs S1-S3). The two subjects shown here are sufficient to illustrate the similarities and differences between the datasets. Results across all four subjects were consistent with the modelling study.

Firing-Rate Profiles for Total EMG Spikes and Relation to Conditioned NM Responses

Previous analysis of retractor bulbi EMG [Lepora, 2007 #8710] showed that during the production of conditioned responses the firing-rate profiles for total EMG spikes have a particular shape that gradually rises from its onset, reaches a peak, then gradually falls to its offset (representative record shown in Fig. 4A, solid line). The peak times of the firing-rate profiles for individual trials are similar, roughly 50-100ms before US-onset. The shapes of the firing rate profiles across all trials can be well fitted by Gaussian functions (Fig. 4A, dashed line), as explained in METHODS.

Figure 4 about here

The conditioned NM response also has a stereotyped shape, with a steep rise from onset to its peak, and then a gradual fall back towards zero displacement (Fig. 4B, black line). Separate trials have a similar latency-to-peak time that coincides with US-onset. The NM response profiles can be generated from the corresponding total EMG spike-rate profiles by passing the latter through a first-order linear differential equation

$$F_{EMG} = Ky + R\frac{dy}{dt} \tag{15}$$

where F_{EMG} is EMG spike firing rate, y is NM position, dy/dt is NM velocity and K and R are constants related to the elasticity and viscosity respectively of the overall system. This system is equivalent to a first-order filter with time constant R/K of approximately 200ms and with gain fixed across all trials of each dataset (Figs 4B and C). Thus, analysis of total EMG-spike firing rates in relation to conditioned

NM response profiles suggests that the nictitating-membrane plant (retractor bulbi muscle, globe, Harder's gland and membrane) behaves effectively as a simple linear system, even though its complicated anatomical structure would incorrectly suggest more complicated dynamics.

Peak EMG Amplitude is Proportional to Peak Conditioned NM Response

Figure 5 about here

The analysis referred to above does not address the issue of motor-unit recruitment, which modelling studies [Mavritsaki, 2007 #8358] suggest would make an important contribution to allowing the plant to behave linearly. To address this issue, we analyse the properties of EMG spike amplitude. As can be seen from Fig. 5, peak EMG spike amplitude is related to peak conditioned response amplitude in a roughly linear manner over the range of response amplitudes studied (up to ~6 mm). Insofar as EMG spike amplitude is related to motor-unit strength (Discussion), these results are consistent the view that conditioned NM response amplitude is controlled by recruiting motor units of increasing strength, at least for the range of response amplitudes investigated.

A previous study found that peak conditioned response amplitude linearly relates to peak EMG spike-rate over the same range of response amplitudes [Fig. 5, Lepora, 2007 #8710]. Therefore peak EMG spike-rate and peak EMG spike amplitude are also related in a roughly linear manner. The precise relation between EMG spike amplitude and EMG spike-rate will be qualified over the next few sections, to suggest the pattern of motor unit recruitment involved in controlling the conditioned NM response. Because the temporal profiles of EMG spike-rate and NM conditioned response amplitude are related by the linear differential equation (15), this motor unit recruitment strategy will be more complex than just depending on the position of the conditioned response.

Firing-Rate Profiles for EMG Spikes of Different Amplitudes

Subsequent more detailed analysis of EMG spike amplitudes showed that spikes of different sizes fired in fixed relation to one another. As described in METHODS, EMG spikes were partitioned into 5 amplitude classes, and representative firing-rate profiles for those classes are shown in Fig. 6.

Figure 6 about here

Four regularities of the retractor bulbi EMG are illustrated in these records. First, larger spikes only appear in conjunction with larger conditioned responses, consistent with the results shown in Fig.

5. Secondly, when larger spikes do appear, they are always preceded and succeeded by smaller spikes (see also Fig. 1). Thirdly, when spike firing rates are compared across trials, the most prominent feature is that the firing rates of the spike amplitude classes change in step with each other. Finally, just as for overall spike frequency (Fig. 4A), the frequency profiles for individual spike classes can also be fitted by Gaussian functions. Note that the EMG amplitude classes gradually increase in amplitude between the trials shown, as is evident in a later plot of the firing rates for each spike amplitude class across all trials (Figs 8A,D)

The Gaussian fits to the spike rates are convenient because they allow the firing-rate profile for each spike-amplitude class *k* to be described by just three parameters: a mean time of spike occurrence μ_k (which equals the time of peak firing for a Gaussian profile), a measure of profile width σ_k, and the peak firing rate h_k (METHODS, equation (8)). This allows the regularities outlined qualitatively above to be described quantitatively in terms of those parameters (Fig. 7). Thus, (i) the mean spike times μ_k for all the classes are timed approximately 50ms before US onset (Fig. 7A,D), (ii) the firing widths σ_k decrease linearly with spike amplitude to zero value at maximum spike amplitude $\varepsilon_{\max}$ (Fig. 7B,E), and (iii) the peak firing rates h_k decrease exponentially with spike amplitude (Fig. 7C,F). These relations can be summarized by three equations

$$\mu_k = \mu, \qquad \sigma_k = l\left(\varepsilon_{\max} - \bar{\varepsilon}_k\right), \qquad \frac{h_k}{h_1} = \exp\left[-u\left(\bar{\varepsilon}_k - \bar{\varepsilon}_1\right)\right], \tag{16}$$

where *l* and *u* are an empirical gradient and exponent respectively (values shown in Fig. 7) and $\bar{\varepsilon}_k$ is the midpoint amplitude for the spikes in amplitude class *k*.

Figure 7 about here

Although the relations in (16) give good fits to the data shown in Fig. 7, there is still an appreciable amount of scatter around the lines of best fit. This arises partly from random variations in the timing of the conditioned responses themselves [references in \Lepora, 2007 #8710`, ;Kehoe, 2008 #9014], which give rise directly to variations in the timing of the inferred motor commands [Lepora, 2007 #8710`, Figs 11, 12]. For example, the time to peak conditioned NM response amplitude is known to vary randomly from trial to trial, as is evident in the variation of the Gaussian means in Figs. 7A, D. However, a second source of scatter comes from pooling data across different conditioned-response amplitudes. For example, it can be seen from Fig. 6 that the width of the best-fit Gaussian

increases with response amplitude for a given amplitude class. This source of scatter can be reproduced by the deterministic common-drive model described below

Relation to Total-EMG Spike Rate

Because of these regularities in the structure of the retractor bulbi EMG, the firing-rates of each individual amplitude class are related to total spike rate in a systematic manner. This is shown in Fig. 8, with firing rates calculated over 50 ms intervals as described in Methods.

Figure 8 about here

The firing-rate for each individual amplitude class is approximately linearly related to total spike firing rate (Fig. 8A,D). The lines of best fit vary with amplitude in two ways. First, the intercept with the x-axis, which corresponds to the total-spike rate at which spikes of the amplitude class appear, increases approximately linearly with spike amplitude (Fig. 8B,E). This corresponds to the qualitative observation that spikes appear and disappear in strict order of amplitude (Fig. 6). Secondly, the gradients of the lines decline with amplitude (Fig. 8C,F), reflecting that high-amplitude spikes always fire more slowly than smaller ones (Fig. 6). This decline is fitted well by a hyperbolic relation, which is consistent with an exponential distribution of motor unit thresholds (modelling section below).

These regularities can be summarized as two equations

$$\bar{b}_k = m\left(\bar{\varepsilon}_k - \theta_0\right), \qquad g_k = \frac{g_1}{1 + v(\bar{\varepsilon}_k - \bar{\varepsilon}_1)}, \tag{17}$$

where the gradient *m* and *v* are empirical parameters (values given on appropriate panels of Fig. 8), $\bar{\varepsilon}_k$ is the midpoint spike amplitude for the spike amplitude class *k* defined in equation (3) and g_k is the gradient of the class versus total-spike rate line.

Simulated EMG Records

The simulated EMG records produced by the common-drive model (Fig. 1) were analyzed in the same way as the actual EMG records described above. The model was used to generate EMG records for 10 different peak input current amplitudes equally distributed over the range 0-4 nA (Methods). To aid comparison with results from the EMG data analysis, the model results are shown for subjects RB1 and RB4 in Figs 6-8 and for subjects RB2 and RB3 in supplementary material (Figs S1-S3).

Properties of Simulated Amplitude Classes

Model EMG spikes were partitioned into 5 amplitude classes in the same way as the recorded spikes. This procedure resulted in a firing rate $\overline{f}_k(t)$ for each of the five amplitude classes.

Results of the simulation (Figs 6G-L) are in good agreement with the experimental data, both qualitatively, as comparison with the experimental data indicates (Figs 6A-F), and quantitatively (see below).The four regularities observed in the experimental data are all present in the simulated records: (i) larger spikes appear only in conjunction with larger input currents (corresponding to larger conditioned response); (ii) when they do appear, larger spikes are always preceded and succeeded by smaller spikes; (iii) when firing rates are compared across trials, the most prominent feature is that the firing rates of the spike amplitude classes change in step with each other; (iv) the spike-rate profiles for individual amplitude classes can be fitted by Gaussian functions.

Describing these Gaussian fits in terms of the mean time of spike occurrence, profile width, and the peak firing rate leads to the three quantitative relations (16) for the simulated datasets that were obtained previously for the experimental datasets In particular: (i) the time of peak firing is the same for all amplitude classes (Figs 7G,J; first relation in (16)), (ii) the widths of the Gaussian fits to firing-rate decrease linearly with spike amplitude to zero value at maximum spike amplitude ε_{max} (Figs 7H,K; second relation in (16)), and (iii) the peak firing rates of the Gaussian fits decrease exponentially with spike amplitude (Figs 7I,L; third relation in (16)).

Both simulated and experimental data show scatter around the lines of best fit. In the case of the experimental data, some of this is caused by random variability that is not present in the modelled data. However, there is also variability that is common to the two sets, which appears to arise from lumping together EMG records corresponding to different amplitudes of conditioned response. The similarity of the scatter patterns in experimental (Figs 7B,E) and simulated data (Figs 7H,K) provides further support for the view that the patterns observed in the experimental data are consistent with a common-drive mechanism for generating conditioned responses.

Relation to Simulated Total-EMG Spike Rate

The experimental results also showed that the firing-rates of spikes of different amplitude were related to the total-spike firing-rate in a systematic manner (Fig 8).

It can be seen that the general pattern of simulated results (Figs 8G-L) are similar to the experimental results (Figs 8A-F). The firing rates for each amplitude class are approximately linearly related to total firing rate (Figs 8G,J). The deviation from linearity seen for the lowest-amplitude spike class arises because the firing-rate for each class in the model is linearly related to input current, whereas the relationship between input current and total spike firing-rate is not precisely linear (Fig. 3D) because of recruitment. There are suggestions of a similar curvilinear relation between the firing rate of the lowest amplitude spike class and total firing rate in the experimental data (Figs 8A,D), although these data show scatter not seen in the deterministic model arising from random variability in the actual EMG recordings. The relationship between spike amplitude and threshold for firing, expressed in terms of total spike firing rate, is also approximately linear (Figs 8H,K), again with the slight deviation from linearity arising from the model neuron firing-rate being linearly related to input current, not total spike firing-rate. The corresponding plots for the experimental data also show approximately linear relations (Figs 8B,E), although the scatter is too great to observe any small systematic deviations from linearity. Finally, the relation between the firing-rate gradient and spike amplitude from each class is fitted well by a hyperbolic function (Figs 8I,L), as expected from an exponential relation between motoneuron number and threshold (Fig. 3), and as observed in the experimental data (Fig 8C,F).

The relations apparent in Figs. 8G-L can be summarized by the quantitative relations (17) found to describe the experimental data.

Model Robustness

Most of the parameters that were varied to fit data sets RB 1-4 related to particular features of the individual data, rather than central aspects of the model itself. To assess the robustness of the model, the effects of varying the main model parameters (equations (11) and (12)) were therefore investigated.

(i) Number of motor units n. Changing n from its baseline value of 100 altered the total- and class-firing rates equally, which rescaled h_k and b_k in equations (16) and (17) while keeping the form of the overall relations shown in Figs 7 and 8. If the number of units was reduced below ~20 the fits to relations (16) and (17) were degraded by discretization errors in separating the units into spike amplitude classes. Model behavior is therefore robust to changing motor unit number provided a reasonable motor unit number is considered.

(ii) As explained in Methods, the magnitude of the input current *I(t)* is determined by the assignment of a maximum value to the input current (I_{max}) that produces the maximum NM extension. Once I_{max} is fixed and a value also given to R_{max}, the highest rheobase threshold in the motoneuron pool, then the motoneuron gain *G* is also determined (Methods). The value of R_{max} in fact determines how much of the force produced by the muscle is produced by recruitment and how much by rate coding. The linear relation between EMG spike amplitude and peak conditioned response amplitude observed for the experimental data (Fig. 3) indicates that for each of the modelled data sets recruitment continues throughout the amplitude range, that is $R_{max} > I_{max}$. With this restriction the overall pattern of simulated EMG results is insensitive to the value of R_{max} (and corresponding value of *G*) provided, provided the sampling parameter *p* is tuned appropriately to match a given experimental dataset. This was demonstrated in simulation (results not shown), but can also be seen directly from the definition of the model because the firing rates of all amplitude classes scale by the same amount on scaling *I*(t) and R_i in equation (11).

(iii) The final parameter to be varied systematically was *q*, which determines the precise exponential relation between motoneuron number and threshold (equation (12)). The exponent *q* in the rheobase distribution determines the parameters *u, v* in relations (16) and (17) (see also Figs 11C and 12C) in a complicated manner. We have verified that the model results fit the general form of relations (16) and (17) for *q* values ranging from 1-10.

Additional Observation

Subject RB1 also had EMG electrodes implanted the orbicularis oculi (OO) muscle, so analysis of OO EMG was also possible for this animals. The pattern of results for spikes of different amplitudes was very similar to that seen for the retractor bulbi EMG.

DISCUSSION

The purpose of the present study was to investigate the control of conditioned NM responses, by analyzing and modelling spike amplitude in EMGs recorded from the retractor bulbi muscle during conditioning. Four main features were revealed and quantified: (i) spike amplitude increased with response amplitude; (ii) smaller spikes always appeared before larger spikes; (iii) subsequent firing rates co-varied for spikes of different amplitude, with smaller spikes always firing at higher rates than larger ones, (iv) subsequent firing-rate profiles were approximately Gaussian for all amplitudes, with parameters related to conditioned NM response parameters so that larger conditioned responses were accompanied by larger spikes. These apparently complex features of the retractor bulbi EMG could be reproduced by a simple model of a common-drive based recruitment in the retractor bulbi muscle, consistent with previous suggestions that the control signal for conditioned NM responses codes the topography of the response in a straightforward manner.

Data Analysis: Recruitment and EMG Amplitude

To our knowledge, spike amplitude in the retractor bulbi EMG has not been analyzed systematically in previous studies. The analyses here indicate a number of respects in which the retractor bulbi EMG resembles that of other muscles. One is that small spikes appear before large ones as muscle activation increases. This observation has been made in many studies [see \Goldberg, 1977 #8106, for introduction to earlier literature] [Jabre, 1996 #9121] [Akaboshi, 2000 #9118] [Durkovic, 2006 #9126], and is generally interpreted in the context of the size principle, according to which weak (small) motor units are recruited before strong (large) ones [Henneman, 1981 #3144]. If the amplitude of an EMG spike reflects the amplitude of a motor unit action potential (MUAP), which in turn is related to the number of fibers in a motor unit and/or the dimensions of individual fibers [Goldberg, 1977 #8106] [Henneman, 1981 #3144], then the appearance of small spikes first is consistent with the size principle.

One caveat for this interpretation is that absolute spike amplitude is also heavily dependent on an extrinsic factor, namely electrode type and position. It is relative amplitude that exhibits the robust recruitment effect, which suggests that it is primarily influenced by factors intrinsic to the motor unit, such as the number of fibers it contains [Henneman, 1981 #3144] or the cross-sectional area of individual fibers [Goldberg, 1977 #8106]. The precise effects of intrinsic and extrinsic factors in determining EMG spike amplitude have been extensively discussed and modelled [e.g.\Clamann,

1985 #9135] [Nandedkar, 1988 #9107] [Nandedkar, 1988 #9127] [Fuglevand, 1993 #3371] [Ertas, 1995 #6754] [Akaboshi, 2000 #9118] [Yao, 2000 #5711] [Stålberg, 2001 #9119;Keenan, 2006 #8294;Keenan, 2007 #9106] [Krutki, 2008 #9138]. In general terms, it appears that intrinsic factors are likely to be particularly dominant in small muscles with one type of muscle fiber, such as the retractor bulbi [Lennerstrand, 1974 #5589;Gray, 1981 #5975].

This direct EMG evidence supports a previous conjecture concerning the importance of recruitment in producing conditioned NM responses [Mavritsaki, 2007 #8358]. This study, based on a model constructed earlier by Bartha and Thompson [, 1992 #1698;, 1992 #1702], demonstrated how, in principle, recruitment of motor units in the retractor bulbi muscle could be used to make the NM plant appear more linear to a higher-level controller.

Data Analysis: Common Drive

A second respect in which the retractor bulbi EMG resembles that of other muscles concerns the relationship between the firing patterns of motor units. First, the firing patterns of different amplitude classes co-varied, and secondly small spikes always fired at a rate higher than that of large spikes (Figs 6, 8). This ensemble behavior, sometimes termed an 'onion skin' pattern, has been observed in other muscles and interpreted as evidence in favor of the common-drive method of muscle-force control [De Luca, 1982 #9122;De Luca, 1982 #9123;Masakado, 1995 #9137;Jabre, 1996 #9121;De Luca, 1996 #3706;Sauvage, 2006 #8496]. The key feature of this method is that all motoneurons in the appropriate pool receive the same synaptic drive from a higher-level controller [De Luca, 1994 #2209], so that the differences in firing rates between motor units are determined primarily by motor-unit properties (and are, as a consequence, highly regular).

The patterns of spike firing found in the retractor bulbi therefore offer a potentially important clue about the nature of the control signal sent to the motoneuron pool for conditioned NM responses. They are consistent with a single-valued command for globe retraction that is sent to all the motoneurons equally, in contrast to the multiple signals apparently sent to the extraocular muscles for control of static eye rotation [McCrea, 1986 #2700;Fuchs, 1988 #430;Dean, 1997 #4171;Hazel, 2002 #5671]. However, the EMG evidence for the common-drive mechanism referred to above typically comes from records in which MUAPs can be assigned reliably to individual units, a process involving sophisticated recording and EMG decomposition techniques [e.g. \Stashuk, 2001 #6665]. The data here are clearly different in that (i) only spike amplitude is used, a variable highly influenced by

extrinsic factor especially when spikes run together in interference patterns [e.g. \Lewicki, 1998 #6645], and that (ii) spikes are assigned to classes not to individual MUs. The fact that the patterns of EMG spike activity found here resemble those obtained when individual MUAPs are identified is thus not by itself conclusive evidence for common-drive control of conditioned eyeblink responses.

There is additional indirect evidence in favour of a common-drive mechanism. The pattern of EMG spike amplitudes found for the retractor bulbi muscle during conditioned responses was also observed for the orbicularis oculi muscle, and when decomposition techniques have been applied to orbicularis EMGs during sustained contractions, they have revealed patterns of MUAPs characteristic of the common-drive mechanism [De Luca, 2006 #9136]. The spike-amplitude patterns observed here are therefore at least consistent with a common-drive command signal. Moreover, overall EMG activity in the orbicularis muscle, which controls the external eyelid, is highly correlated with NM response amplitude during conditioning [McCormick, 1982 #5646;Lavond, 1990 #85;Attwell, 2002 #8264]. It appears that the orbicularis oculi and retractor bulbi pools receive very similar inputs during conditioning, a similarity that could be easily be achieved using the simple, single-valued commands required by the common-drive mechanism.

Nonetheless, it was necessary to demonstrate conclusively whether the patterns of EMG spikes observed in the present study are or are not those produced by a common-drive mechanism. These patterns were therefore modelled explicitly.

Modelling

Comparing the results of data an analysis and modelling (Figs 6-8) shows that the complex patterns of EMG spikes discerned in the data could be well reproduced by a simple common-drive model. An important issue is whether the match between model and data required values of model parameter that were realistic.

Parameter Values

To our knowledge, the intrinsic gains and thresholds of accessory abducens motoneurons in the rabbit have not been measured. However, indirect evidence suggests that the model values for these quantities are generally reasonable. For cat abducens motoneurons, gains range from 20 to 40 Hz/nA, and thresholds from 1.5 to 8.3 nA [Grantyn, 1978 #1523;Dean, 1997 #4171]. The corresponding model values are 20 Hz/nA, and 0 to 7.5 nA. The main problem appears to be that the

model uses motoneurons with lower intrinsic thresholds than are observed experimentally. However, the low values in the model are to some extent uncertain, since the actual time course of the Gaussian motor commands is not measured directly, but instead inferred from the EMG data themselves. Thus, the true value of current threshold at which the lowest threshold motoneuron starts firing is not known. Moreover, there is evidence that the red nucleus, thought to be the immediate source of motor commands for conditioned NM responses [Hesslow, 2002 #7004;Thompson, 2005 #8399] [Robleto, 2008 #8932], contains neurons that fire tonically [Desmond, 1991 #8537]. Given that inputs from the relevant (contralateral) red nucleus are excitatory, tonic drive from the red nucleus would in effect lower the thresholds of accessory abducens neurons. This possibility is considered further below.

A second potential source of concern with regard to model parameter values is the wide range of EMG spike amplitudes. These can be expressed as the ratios of the largest possible spike heights ε_{max} in the model to the threshold spike heights θ_0 (equation (13)), and take the values 27, 14, 50 and 12 fold for datasets RB1-4 respectively. These figures could be consistent with the estimated range of cat RB unit strengths [i.e. 3.5, \Lennerstrand, 1974 #5589] if motor unit EMG spike amplitudes increase faster than their strengths, and some evidence from skeletal muscle suggests this to be the case [Goldberg, 1977 #8106]. It is also likely that the range of motor unit strengths in rabbit retractor bulbi muscle is greater than that in cat, because the rabbit muscle contains three distinct fiber types [Pachter, 1976 #5982] whereas the cat muscle is relatively homogeneous [Alvarado, 1967 #5623;Lennerstrand, 1974 #5589;Crandall, 1981 #1140;Gurahian, 1987 #1145]. Finally, the range of cat RB motor unit strengths cannot be compared directly with the present data because we utilized sums of EMG activity to estimate motor unit strength. For these reasons the range of EMG spike amplitudes used in the model is not inconsistent with current data.

Tonic Inputs to Accessory Abducens Regulate NM Reflex Excitability.

The excitability of accessory abducens neurons, and so the threshold and gain of the NM reflex, will depend upon levels of tonic excitatory and inhibitory inputs. The red nucleus provides a significant excitatory input to the accessory abducens that is phasically modulated in the production of conditioned NM responses [Desmond, 1991 #8537], and is known to be essential for the production of conditioned NM responses [Rosenfield, 1983 #3210;Bracha, 1993 #1715;Robleto, 2008 #8932] consistent with the view that the motor command for conditioned NM responses is sent from the

anterior interpositus nucleus to the accessory abducens nucleus via the red nucleus [Yeo, 1998 #4666;Hesslow, 2002 #7004;Christian, 2003 #7413]

However, tonic excitatory input from the red nucleus to the accessory abducens nucleus will decrease the thresholds of some motoneurons, so inactivation of the red nucleus would be expected to have a secondary effect, namely some reduction in amplitude of unconditioned responses elicited via trigeminal inputs to the accessory abducens. Such amplitude reductions have been reported following inactivations of the red nucleus [Bracha, 1993 #1715] and of the cerebellar interpositus nucleus, which provides excitatory drive to the red nucleus [Welsh, 1989 #8352]. Consistent with this interpretation, elevating red nucleus tonic activity by applying gabazine to interpositus neurons involved in trigeminal reflex blinks increases the amplitude and duration of reflex blinks in the external eyelid system [Chen, 2006 #8467]. In evaluating evidence from studies of the mechanisms and sites for generating conditioned responses, the importance of changes in these tonic modulatory influences must be considered. Excitability changes that lead to changes in the expression or performance of the reflex and conditioned responses must be dissociated to reveal mechanisms specific to learning [Yeo, 1992 #910;Hesslow, 2002 #7004].

Finally, it is important to note that, in addition to red nucleus inputs and trigeminal inputs, accessory abducens probably receive additional modulatory inputs. There is evidence that for a diversity of synaptic types in these motoneurons [Destombes, 1983 #5980], and facial motoneurons receive serotonergic input [Aghajanian, 1980 #9464] that may modify their levels of excitability [e.g.\Hounsgaard, 1986 #3297]. So, even though conditioned responses may be produced by a common drive, there are probably other inputs to accessory abducens motoneurons which could produce effects not modelled here.

Evidence from Motoneuron Firing Rates

The common-drive mechanism for motoneuron recruitment described above predicts the firing patterns of motoneurons during CRs, given that the relationship between total EMG-spike firing rate and CR parameters is described by the simple first-order equation (15). Above its individual threshold, the firing rate for an individual motoneuron will be approximately linearly related to combined NM position and velocity (right hand side of equation (15)).

At present the data required to test this prediction are not available, since the firing rates of motoneurons in the rabbit accessory abducens nucleus during the production of conditioned NM

responses have not apparently been recorded systematically [Lepora, 2007 #8710]. Data are available for cat, but it appears that in this species accessory abducens motoneurons do not fire in relation to CRs, at least for the CSs used in the study [Trigo, 1999 #5297]. In the case of orbicularis oculi (OO) motoneurons in the facial nucleus, we have previously shown that their general firing patterns during both URs and CRs are consistent with equation (15) [Lepora, 2007 #8710, Fig 13]. However, details of individual motoneuron thresholds in relation to eyelid position and velocity are not presented explicitly. Trigo, Gruart and Delgado-Garcia [, 1999 #5297] show linear fits to the firing rates of OO motoneurons as a function of eyelid position during CRs (Fig 16C), but it appears from the fits that the motoneurons would be tonically active when the eyelid is in its resting position. Whether these data are in fact consistent with the common-drive mechanism cannot be determined.

As mentioned above, the first-order model derived by Lepora et al. (2007) could be used to fit firing-rate data for OO motoneurons for both CRs and URs. Analysis of the relationship between EMG and UR parameters was not possible in the present study, because most of the trials used a shock US with consequent interference with the EMG record from the shock artefact. The interesting question of whether URs are also controlled by a common-drive mechanism, or in some other manner [Bartha, 1992 #1698;Bartha, 1992 #1702], remains to be addressed.

Control Signal for Conditioned Eyeblink Responses

The results from the present modelling study suggest that, as conjectured previously [Mavritsaki, 2007 #8358;Lepora, 2007 #8710], conditioned NM responses are generated by a relatively simple motor command that is converted into the appropriate pattern of motoneuron firing by the recruitment properties of the motoneuron pool. This idea of a simple command is consistent with evidence that very similar signals for conditioned responses are sent to both retractor bulbi and orbicularis oculi muscles [McCormick, 1982 #5646;Lavond, 1990 #85;Attwell, 2002 #8264]. It appears that, despite the complexities of the NM plant, conditioned NM responses are in fact relatively easy to control because the plant has been effectively simplified. The creation of a simplified "virtual plant" probably uses a combination of mechanisms (see Discussion in [Lepora, 2007 #8710]) in addition to the recruitment process proposed here. The overall result is that a common-drive Gaussian signal sent to the accessory abducens nucleus is straightforwardly related to NM response parameters. In electrophysiological investigation of the mechanisms underlying classical conditioning using the NM

response system, this straightforward relationship should simplify parts of the analysis, especially at control sites with relatively direct, oligosynaptic projections to the motoneuron pool.

Although the firing rate properties of eyeblink neurons resemble those of ocular motoneurons to some extent [Trigo, 2003 #7192], recruitment seems rather different in the two systems. The behaviour of ocular motor neurons appears not to result from a common-drive mechanism, but rather from differences in synaptic drives to different motoneurons [Dean, 1997 #4171;Hazel, 2002 #5671]. The more complex commands required by the oculomotor system probably reflect both its structure, with multiple types of motor unit, and the variety and precision of the responses it controls with respect to both eye velocity and position [e.g. \Büttner, 2006 #8220]. In contrast, the role of the accessory abducens and orbicularis oculi motoneurons is much more straightforward, since their only job is to produce rapid movements of the nictitating membrane and eyelid lid, followed by a return to their starting position at the end of the blink.

In terms of wider applicability, however, the common-drive mechanism suggested here for conditioned NM responses has been described for numerous other skeletal-muscle responses [e.g.\De Luca, 1982 #9122;De Luca, 1982 #9123;Masakado, 1995 #9137;Jabre, 1996 #9121;De Luca, 1996 #3706;Sauvage, 2006 #8496]. This suggests that a general principle of making movement control as simple for higher-level neural structures may be followed when possible, and indeed a variety of mechanisms for creating simplified "virtual plants" have been described [e.g. \Nichols, 1976 #7889;Mussa-Ivaldi, 1994 #8576] [Demer, 2006 #8278]. In this context, the method of analyzing EMG records described here may be convenient for identifying putative common-drive mechanisms for movements not so far investigated.

Role of Cerebellum

The role of the cerebellum in the production of CRs has been the subject of extensive investigation and dispute [Hesslow, 2002 #7004][Thompson, 2005 #8399]. It appears to be generally agreed that in the specific case studied here, namely delayed conditioning of the NM response in rabbit, the CR is controlled by signals sent to the accessory abducens nucleus from the anterior interpositus nucleus via the red nucleus [Hesslow, 2002 #7004][Thompson, 2005 #8399]. The question then arises whether cerebellar output could deal with the complexities of the NM plant (Introduction). The present results suggest a mechanism that would allow the parameters of cerebellar output signals with a Gaussian temporal profile to be related simply to the parameters of the CR [Lepora, 2007

#8710]. This mechanism may also be used for CRs of the eyelids, given the evidence referred to above that the control signals for NM and external eyelid CRs in delay conditioning in rabbits are similar. A detailed model of the eyelid plant is needed to indicate how it too might be linearised.

It is important to note, however, that the nature and origin of the control signals used in trace conditioning, which depends upon forebrain structures such as the hippocampus, and in other animals such as cats and mice [Delgado-García, 2006 #8397], remain to be determined. It is possible that EMG analysis of the kind used here will be helpful for elucidating whether, in accordance with the general principle of plant simplification outlined above, the common-drive mechanism for motoneuron recruitment is used in these cases as well.

Grants

This research was supported by the United Kingdom Biotechnology and Biological Research Council (Grant BBS/B/17026 under the Integrative Analysis of Brain and Behaviour Initiative), the Wellcome Trust (VIP award to N. Lepora), and National Eye Institute (Grant EY07391 to C. Evinger).

References

Figure 1

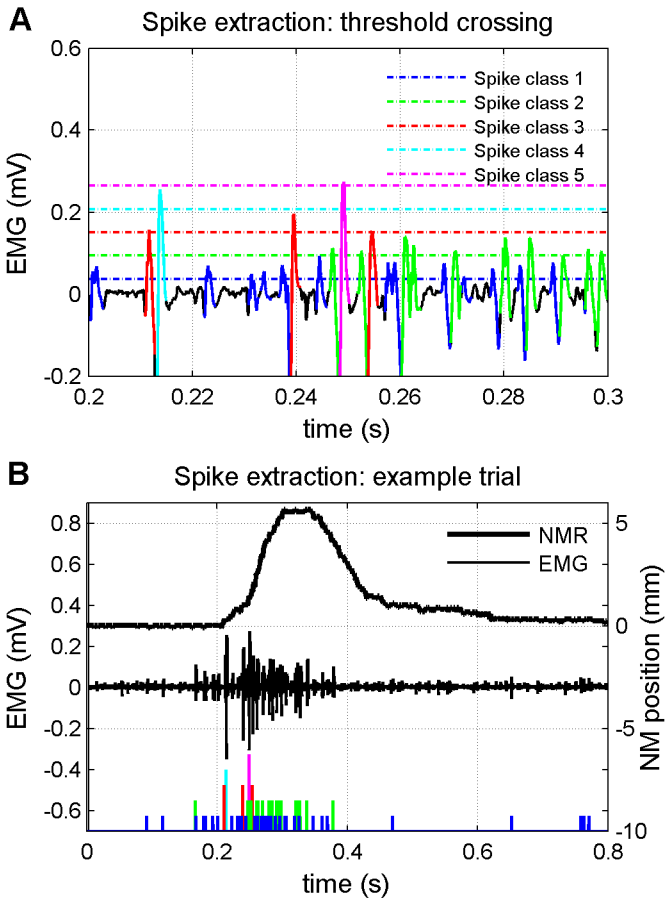

Example of spike extraction and classification for EMG of retractor bulbi muscle (subject RB4).

A: A portion of EMG record shown with expanded time base to illustrate threshold crossing criterion for spike extraction and classification for five spike amplitude classes.

B: Entire EMG record for a conditioned-stimulus alone trial (middle trace), showing extracted and classified spikes (bottom trace), and conditioned nictitating membrane response (NMR; top trace). The record is the same as that used in Fig. 1 of [Lepora, 2007 #8710], with panel A shifted by -50ms to show the tallest spikes. (The threshold was erroneously shown at too high a value in that figure, though the correct value of 0.0375mV was used correctly elsewhere in the paper.)

Figure 2

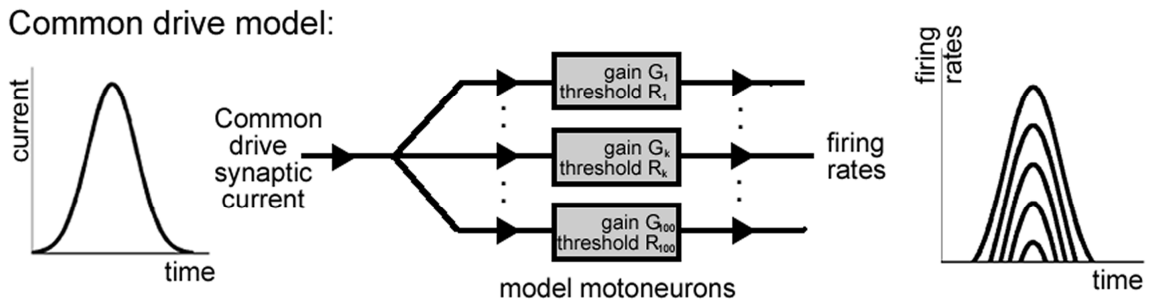

Common drive model of motoneuron firing.

Input to model is the common drive synaptic current, which is distributed equally across 100 simplified model neurons. These model motoneurons have firing rates that are linearly proportional to the input synaptic currents above a threshold *R* (the rheobase current) with gain G. Each model motoneuron is assumed to control a specified population of muscle fibers – the motor unit. Assuming each motor unit generates an EMG spike with characteristic amplitude (here assumed proportional to the rheobase current), these motoneuron firing rates can be used to simulate an EMG record for the muscle in response to the common drive current.

Figure 3

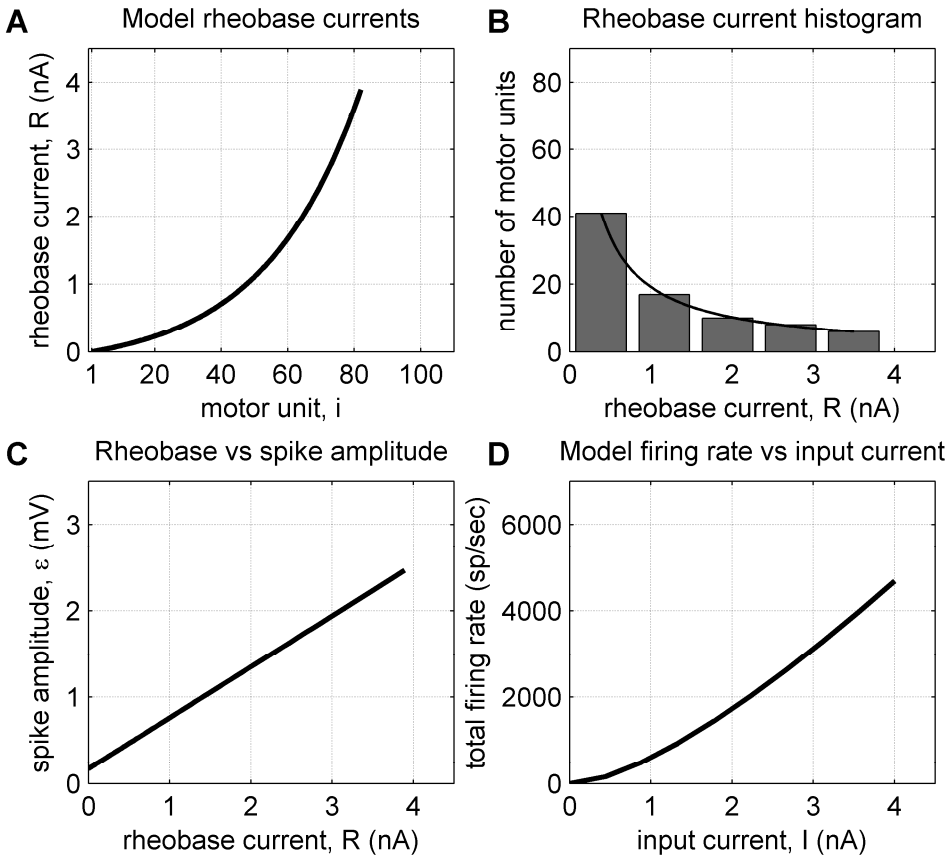

Properties of the model of the motoneuron pool with parameters derived from the RB1 dataset (details in Methods).

A. Exponential relation (equation (12)) between motoneuron threshold (rheobase current) and the index *i* of the motor unit, numbered from 1 (smallest threshold) to 100 (largest threshold). For the RB1 dataset the largest input current was 4 nA, so that neurons with a rheobase higher than this value were not recruited.

B. Distribution of motor units with respect to rheobase current, derived from the relation shown in A. The histogram indicates the number of units in each of 5 equal bins over the range of rheobase currents 0-4nA. The exponential relation in equation (12) gives a hyperbolic distribution of motor unit numbers (best-fit hyperbola for a histogram with five intervals $y = 41/\left(1+1.86\left(R-0.4\right)\right)$ shown as black curve on plot), as expected theoretically by integrating relation (12) over motor unit number.

C: Linear relation between rheobase current and EMG spike amplitude. The *x*-intercept of this linear relation is the minimum threshold θ_0 = 0.17mV for EMG spike detection in dataset RB1.

D: Relation between common drive input current and total motoneuron firing rate from model equations (11) and (12). Note the weak deviation from linearity for small input currents.

Figure 4

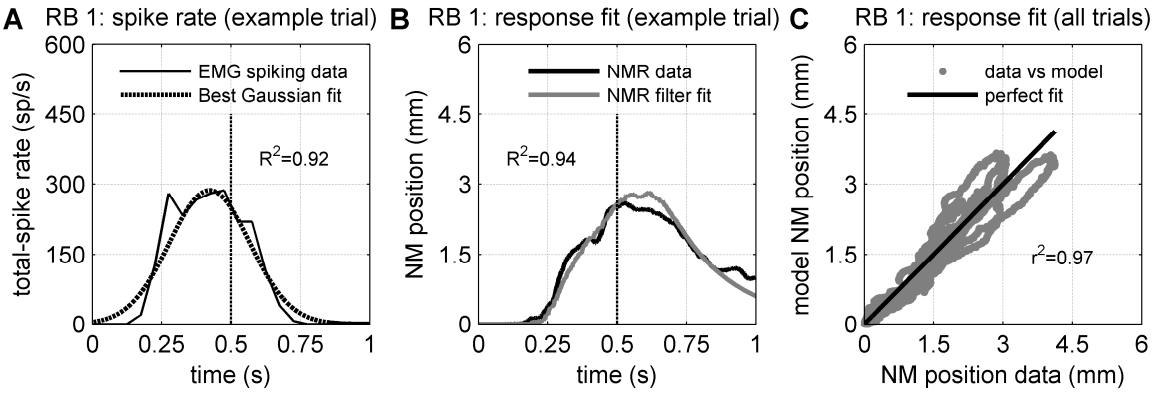

Representative EMG spike-rate profile and CR profile for subject RB1.

A: Temporal profile of EMG total-spike rate and its best-fit Gaussian profile. CS onset is at time zero and US onset is denoted by the dotted vertical line. The trace is the mean of 3 EMG spike-rate profiles.

B: Temporal profile of conditioned NM response and the best-fit derived from a linear filter model (equation 1). The two traces are means over 3 responses corresponding to the records averaged over in panel A.

C: Predictions from linear-filter model plotted against data points for all conditioned NM responses for RB1 (sampled every 1ms for each response). The close match shows the linear model is a good fit to the data.

Figure 5

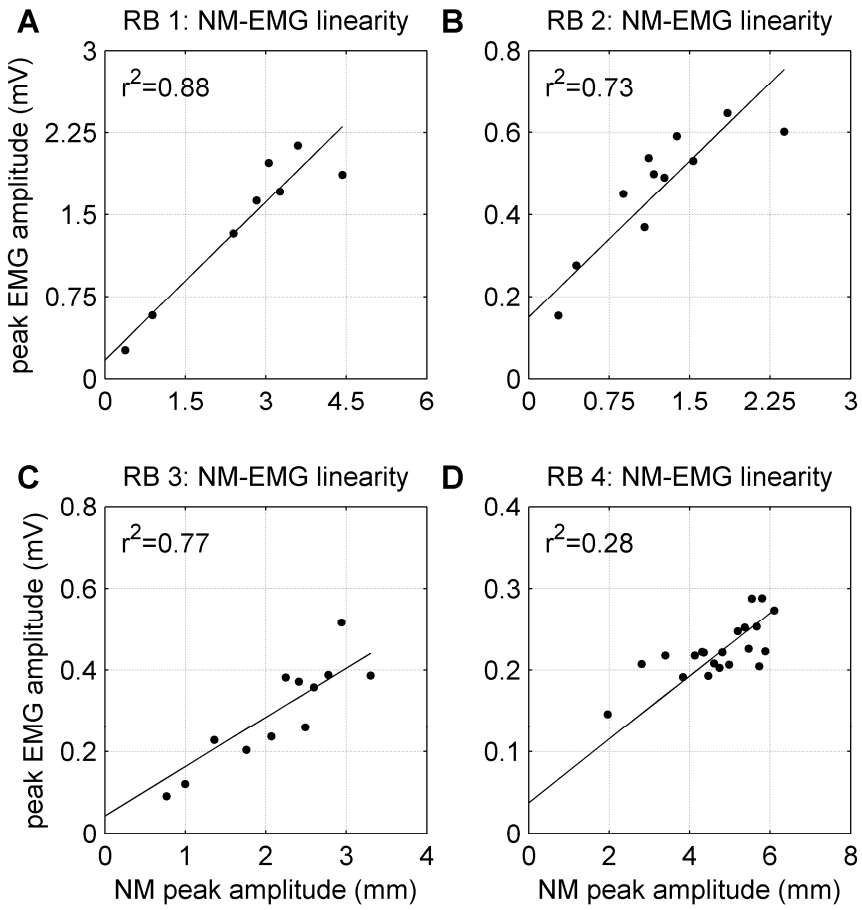

Peak EMG amplitudes plotted against peak conditioned NM responses for subjects RB1-4.

A-D: Each data point is a mean of 3 EMG records of similar conditioned-response peak amplitude (hence the peak values appear less than those in Table 1). The relationship between peak EMG amplitude and peak NM amplitude is approximately linear for all subjects (best linear fit constrained to pass through EMG-spike threshold θ_0 at zero response amplitude). There is no evidence for saturation of EMG spike amplitude over the range of response amplitudes available.

Figure 6

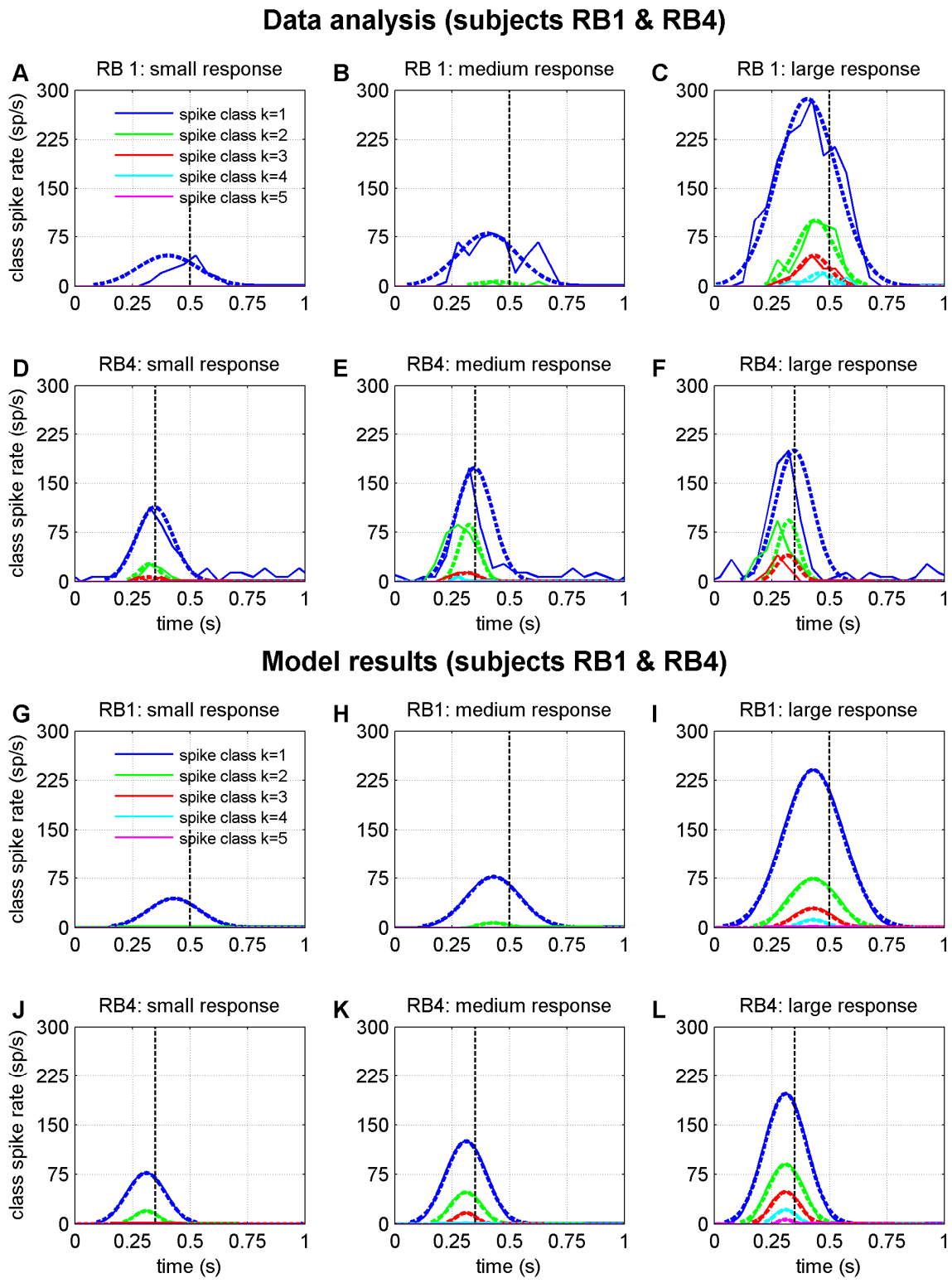

Recorded and simulated EMG spike-rate profiles for different spike-amplitude classes, corresponding to conditioned NM responses of different amplitude for subjects RB1 and 4.

Panels A-F: EMG data. Each trace is a mean of 3 EMG firing rate profiles for spike amplitudes partitioned into 5 classes. An individual profile was calculated every 50ms as the firing rate of the spikes in a given amplitude class in a surrounding 50ms bin. In each panel, CS onset is at time 0, and US onset is denoted by a dotted vertical line. Gaussian curves were fitted to traces (dashed lines).

Panels G-L: Model EMG results. Model results are generated for ten model trials with peak input currents I_0 ranging from zero to 4 nA. The small, medium and large responses are the second, fourth and ninth model trials respectively. All other simulated conditions are as for the data traces. Note that because the Gaussian fits (dashed lines) well approximate the model results (solid lines) the two curves almost overlay.

Figure 7

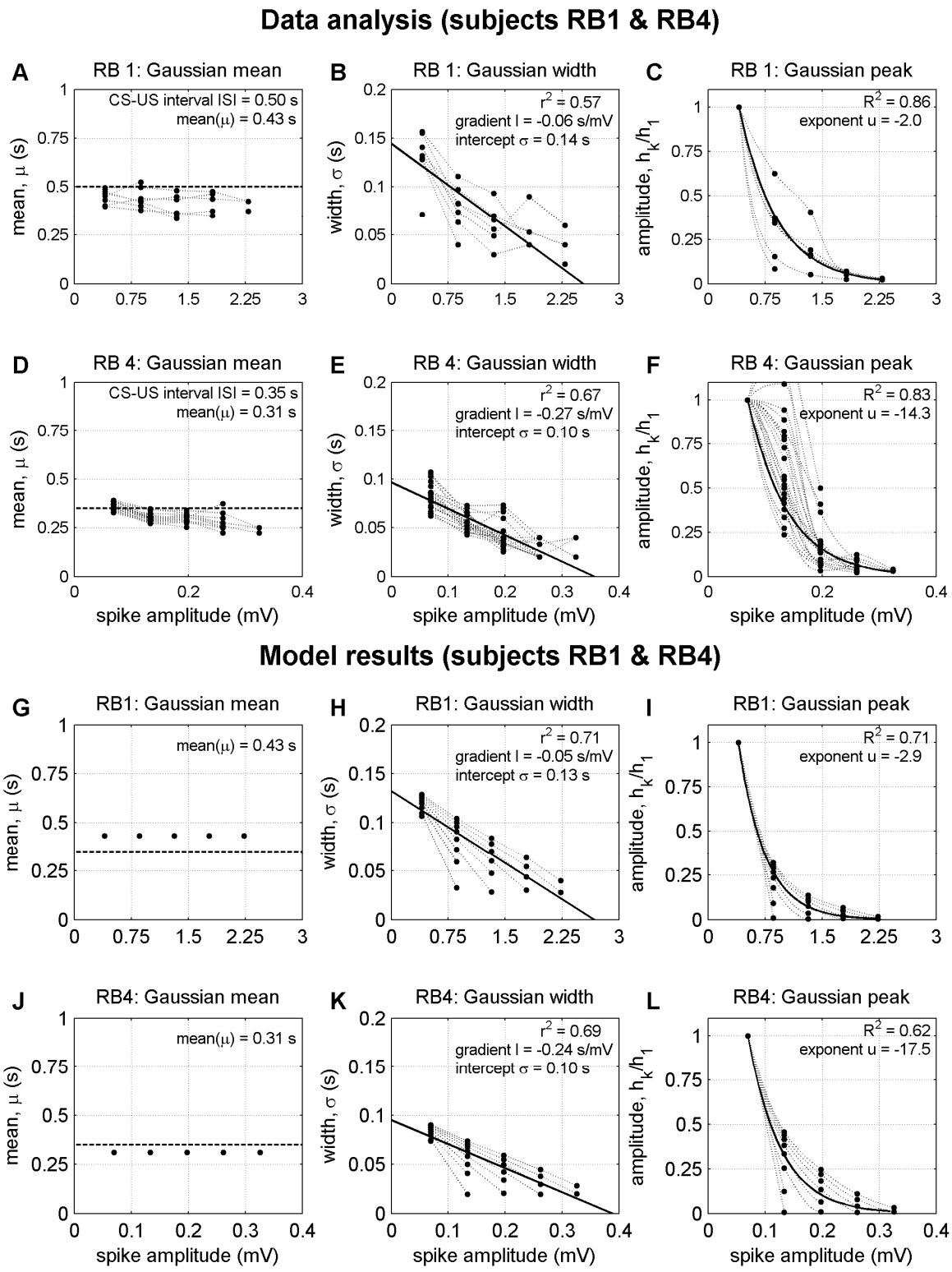

Parameters of Gaussian fits to recorded and simulated EMG spike-rate profiles as functions of spike amplitude for subjects RB1 and 4.

Panels A-F: EMG data analysis. Data points correspond to the mean (panels A, D), width (panels B & E) and peak firing rate (panels C & F) of the Gaussian fits in panels A-F of Fig. 6 for each spike-amplitude class, plotted against the central value of spike-amplitude for that class. Dashed lines join data points from trials with similar values of conditioned response amplitude (results averaged over three trial batches). US onset is denoted by the dotted horizontal line on panels A & D. The best fit line and r^2 value (where r is the correlation coefficient) is shown on panels B & E. The best fit exponential and it r^2 value is shown on panels C & F. The ratio of peak firing rates h_k/h_1 is used in Fig. 7C to show the dependence of peak class-firing rate on spike amplitude independently of the peak total-firing rate.

Panels G-L: Model EMG results. Results generated similarly to the EMG data, for the simulated EMG results in panels G-L of Fig. 6.

Figure 8

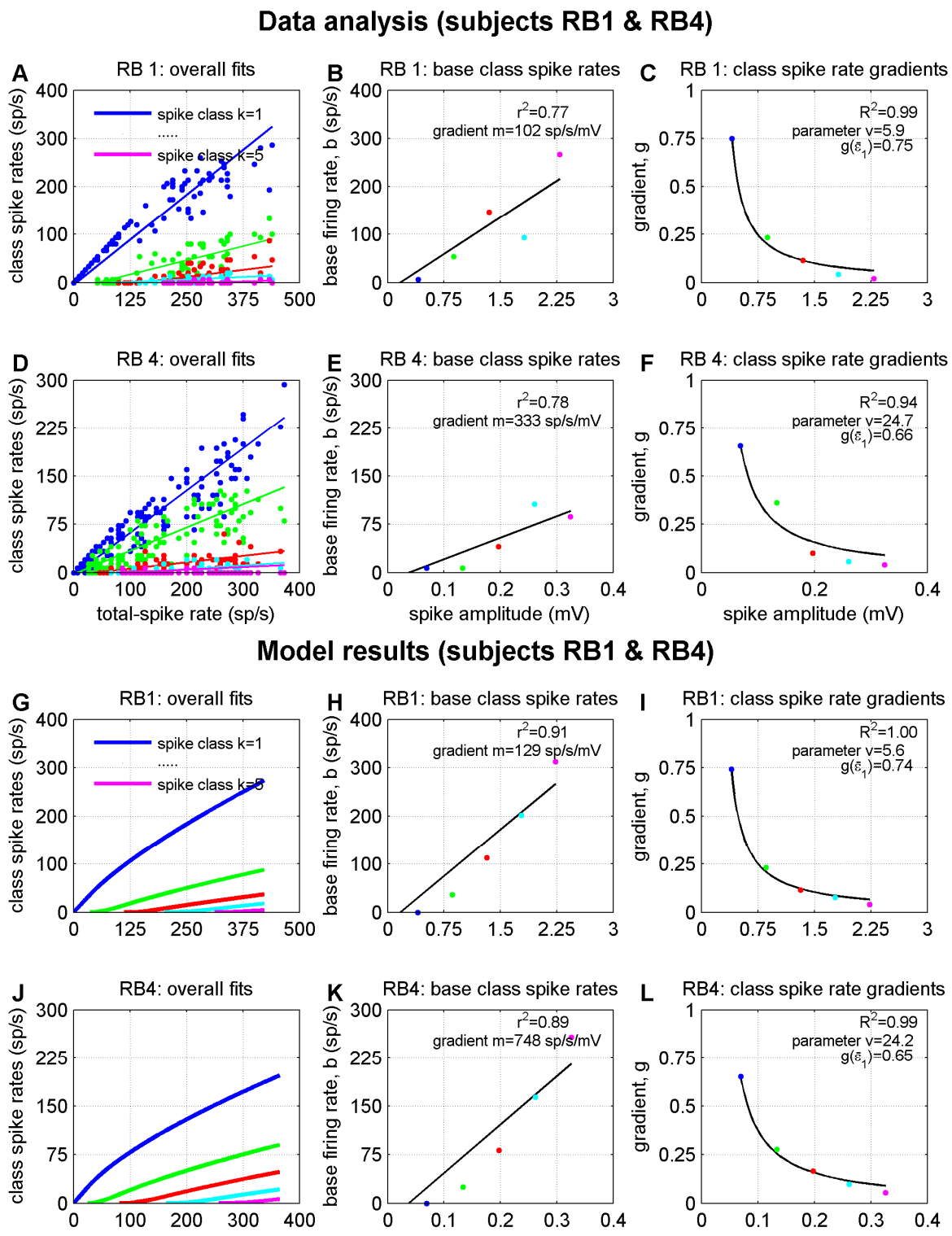

Recorded and simulated change in class spike rate with total-spike rate for subjects RB1 and 4.

Panels A & D: Class spike rate plotted against total-spike rate sampled at 50 ms intervals. For each spike amplitude class, this relation is approximately linear (linear fits denoted by the solid lines; data by the points).

Panels B & E: Base firing rates (total-spike rate where a class spike rate becomes non-zero) plotted against the central spike amplitude for each of the spike amplitude classes in panels A & D. The solid line is the best linear fit to this data that passes through zero base firing rate when the spike amplitude equals the EMG threshold θ_0.

Panels C & F: The gradients of the best-fits in panels A & D plotted against the central spike amplitude for each spike amplitude class. Hyperbolas (see equation (17)) were found to give good fits to these data.

Panels G-L: Model EMG results. The analysis of the simulated EMG records is the same as that for the EMG data in panels A-F.

Table 1

subject	*Spike amplitudes*		*total spike rate Gaussian fits*				*NM response*
	threshold θ_0 (mV)	maximum ε_{max} (mV)	median center μ (s)	median width σ (s)	peak range h (sp/s)	median fit R^2	amplitude range y (mm)
RB 1	0.17	2.53	0.45	0.13	0-440	0.92	0-4.4
RB 2	0.15	0.75	0.29	0.06	0-220	0.94	0-2.4
RB 3	0.0275	0.67	0.36	0.10	0-450	0.83	0-3.3
RB 4	0.0375	0.36	0.39	0.07	0-370	0.82	0-6.1

Parameters describing the observed and fitted EMG spike rate profile and CR profile for subjects RB1-4.